

Synergistic Roles of Single Co Atoms and Co Nanoparticles for the Hydrodeoxygenation and Ring Hydrogenation Reactions

Song Han,^{||} Ruijie Gao,^{||} Ming-Shuai Sun, Yan Zhou, Wen-Ting Chen, Xixi Liu, Jingzhong Qin, Duan-Jian Tao,^{*} and Zehui Zhang^{*}



Cite This: *J. Phys. Chem. C* 2023, 127, 14185–14196



Read Online

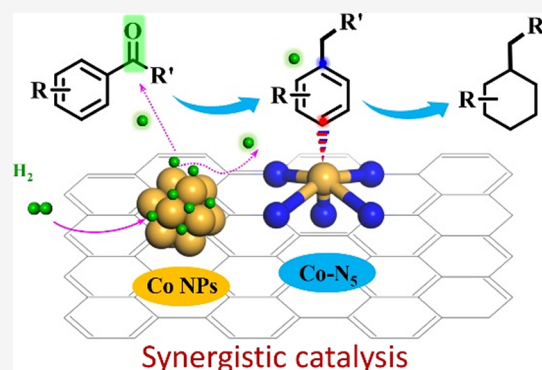
ACCESS |

Metrics & More

Article Recommendations

Supporting Information

ABSTRACT: Because of the highly inert aromatic ring, the hydrodeoxygenation and subsequent ring hydrogenation reactions of aromatic ketones into high-energy-density liquid hydrocarbons remain a great challenge even over noble metal catalysts. Herein, the heterogeneous cobalt catalysts composed of metallic Co nanoparticles and single Co atoms with Co–N₅ motifs were found to display excellent activity in the simultaneous hydrodeoxygenation of C=O/C–OH bonds as well as the hydrogenation of the aromatic ring into high-energy-density liquid hydrocarbons, where single Co atoms served as the Lewis acid sites to activate the C=O/C–OH bonds as well as the aromatic ring, and metallic Co nanoparticles activated H₂ molecules. Experimental data as well as DFT calculation further revealed that the single Co atoms activated the inert aromatic ring by changing the electron density of each carbon in the aromatic ring and thus facilitated the hydrogenation of the aromatic ring with a much lower energy barrier (1.14 vs 1.96 eV without the single Co atom sites).



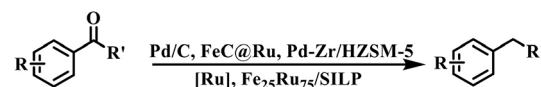
1. INTRODUCTION

Catalytic reduction reactions with H₂ represent one kind of the most important organic transformations to access high-value fine chemicals, pharmaceuticals, as well as high-energy-density liquid fuels.^{1–3} Among the different types of catalytic reduction reactions, catalytic hydrodeoxygenation reactions have received particular attention, particularly in biomass refinery.^{4,5} Many biomass-derived molecules are highly oxidized,⁶ and thus the removal of surplus oxygen via the hydrodeoxygenation reaction is key to their usability as fuels, which would reduce the dependence on fossil fuel resources.^{7,8}

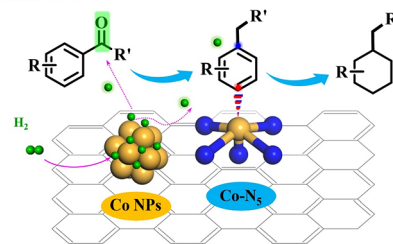
Hydrodeoxygenation of lignin-derived aromatic ketones was mainly performed over noble metal catalysts, such as Fe₂₅Ru₇₅ in solid ionic liquid phase (Fe₂₅Ru₇₅/SILP),^{9,10} and heterogeneous Pd catalysts^{11,12} (Scheme 1, reaction A). Some noble metal catalytic reactions were even performed under harsh reaction conditions. For example, the hydrodeoxygenation of aromatic carbonyl compounds into arenes over the Fe₂₅Ru₇₅/SILP catalyst was performed at 175 °C and 50 bar H₂.⁹ Apart from the hydrodeoxygenation of aromatic ketones into arenes, it is also important to design the robust catalysts to further promote the hydrogenation of the inert aromatic ring to get saturated hydrocarbons with high energy density. However, it is a great challenge to carry out the simultaneous hydrodeoxygenation of C=O/C–OH bonds and hydrogenation of the aromatic ring over one catalyst. Some catalysts were only active for the hydrodeoxygenation reactions,^{13,14} while some

Scheme 1. Current Methods for the Reduction of Aromatic Ketones

Reaction A (previous works)



Reaction B (this work)



catalysts could only promote the hydrogenation of the aromatic ring.^{15–17} From the green and sustainable viewpoints, it is highly demanded to design heterogeneous non-noble

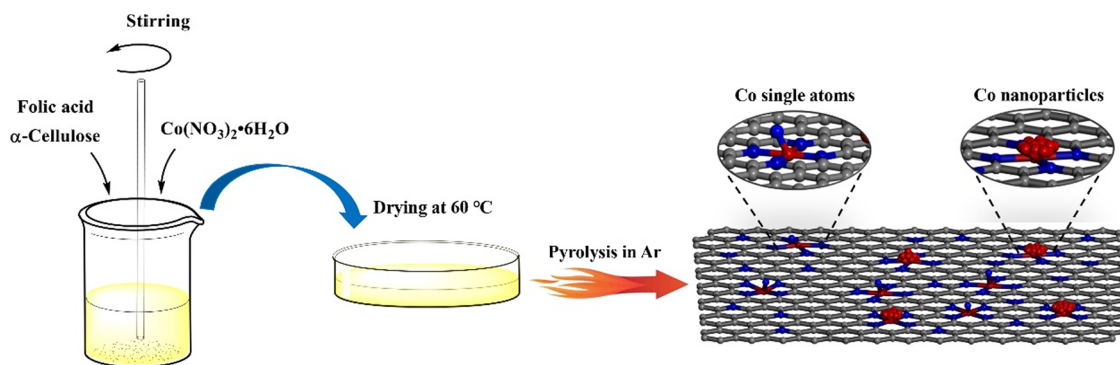
Received: April 8, 2023

Revised: June 29, 2023

Published: July 18, 2023



Scheme 2. Schematic Illustration for the Preparation of Co@NC-T Catalysts



metal catalysts for the simultaneous hydrodeoxygenation of C=O/C–OH bonds and hydrogenation of the aromatic ring to generate cyclohexane derivatives with high energy density under mild conditions.

After an extensive and careful investigation of the reported references on the hydrodeoxygenation of C=O/C–OH bonds and the hydrogenation of the aromatic ring, it is known that Lewis acid sites could activate C–OH bonds to promote the Pd-catalyzed hydrodeoxygenation of C–O/C=O bonds¹³ and the hydrogenation of the aromatic ring over noble metal catalysts.^{18,19} For example, Miyamura and Kobayashi recently discovered that Lewis acid Yb(OTf)₃ could greatly improve the catalytic activity of the heterogeneous rhodium–platinum (Rh–Pt) bimetallic catalyst for the hydrogenation of anilines into cyclohexane amines with an increased conversion from 9 to 89%.¹⁹ Therefore, it is anticipated to design one kind of heterogeneous catalysts bearing Lewis acid sites and metal nanoparticles for the simultaneous hydrodeoxygenation of C=O/C–OH bonds and hydrogenation of the aromatic ring to generate cyclohexane derivatives under mild conditions.

In our previous work, the nitrogen-doped carbon materials were successfully used to stabilize the single metal atoms (M–N_x),^{20–22} metal complex,²³ or metal nanoparticles,²⁴ which demonstrated excellent catalytic performance for some oxidation and hydrogenation reactions. For example, the single Zn atom catalyst bearing Zn–N₄ motifs was robust for the oxidative cleavage of ketones into esters, where the single Zn atoms served as the Lewis acid sites to activate C=O bonds.²¹ Inspired by the fact that some nitrogen-stabilized single metal atom catalysts were prepared by the removal of metal nanoparticles by acid-washing strategy after the pyrolysis of metal–organic complex precursors,^{25–27} herein, the nitrogen-doped carbon-stabilized Co nanoparticles and single Co atoms were successfully prepared by the facile pyrolysis strategy, and they were discovered to be active to promote the simultaneous hydrodeoxygenation of C=O bonds and hydrogenation of the aromatic ring in aromatic ketones to generate cyclohexane derivatives (Scheme 1, reaction B). In addition, the developed catalytic system was also effective for the hydrogenation of N-heteroaromatic ring to access saturated N-heterocyclic compounds as well as the hydrodeoxygenation of aliphatic alcohols and carbonyl compounds into alkanes.

2. METHODS

2.1. Catalyst Preparation. Typically, folic acid (2.68 g) and α -cellulose (3.20 g) were added into 30 mL of deionized water and stirred vigorously for 1 h at room temperature. Then, Co(NO₃)₂·6H₂O (0.90 g) was added into the mixture

and stirred for another 12 h. After the evaporation of water at 60 °C, the yellow composite was placed into a tubular furnace. Then, the tubular furnace was thermally treated with an argon (Ar) flow from room temperature to 600 °C at a heating rate of 2 °C·min^{−1} and then kept at 600 °C for 2 h. Then, the tubular furnace was cooled down to room temperature, and the nitrogen-doped carbon-supported Co catalyst was obtained, which was labeled as Co@NC-600. Similarly, Co@NC-500 and Co@NC-700 were also prepared by the same procedure at the pyrolysis temperatures of 500 and 700 °C, respectively.

NC-600 was prepared by the same procedure as Co@NC-600 without the addition of Co(NO₃)₂·6H₂O. For comparison, Co/NC-600 was also prepared via two steps, including the first step of impregnation of Co(NO₃)₂ into the NC-600 support, followed by the reduction of Co²⁺ into Co nanoparticles with 10% H₂/90%N₂ (v/v) at 600 °C for 2 h. Co@NC-600-AT was prepared by the acid treatment of Co@NC-600 using 1 mol·L^{−1} HCl under 50 °C for 12 h to remove metallic Co nanoparticles.

2.2. General Procedures. In a typical run, acetophenone (0.5 mmol), the Co@NC-600 catalyst (40 mg), and cyclohexane (5 mL) were charged into a 25 mL autoclave with a magnetic stirrer. After the removal of air in the autoclave by the flush of H₂ for 10 min, the autoclave was pressured with 10 bar H₂ and sealed. Then, the autoclave was heated from room temperature to the desired temperature within several minutes, and the reaction was started with a magnetic stirring at 800 rpm. After the reaction, the catalyst was filtered off with an external magnet, and the sample of the mixture was diluted with ethanol and identified by gas chromatography–mass spectrometry (GC–MS) (Thermo Trace 1300 GC-ISO).

3. RESULTS AND DISCUSSION

3.1. Catalyst Preparation and Characterization. The Co@NC-T catalysts were prepared by the simple pyrolysis method (Scheme 2). In brief, the precursor composed of folic acid, α -cellulose, and Co(NO₃)₂·6H₂O was subjected to pyrolysis at three representative temperatures (500–700 °C) under the flow of Ar, and Co@NC-T catalysts were attained, where T represents the pyrolysis temperature. The weight percentage of Co in the Co@NC-T catalysts was determined by inductively coupled plasma optical emission spectrometry (ICP-OES) analysis, which increased with the increase of the pyrolysis temperature, due to the release of much more volatile gases at higher pyrolysis temperatures (Tables S1 and S2). Three peaks with $2\theta = 44.2$, 51.5, and 75.9° were observed in the XRD patterns of Co@NC-600 and Co@NC-700 (Figure S1), assigned to the (111), (200), and (220) crystal planes of

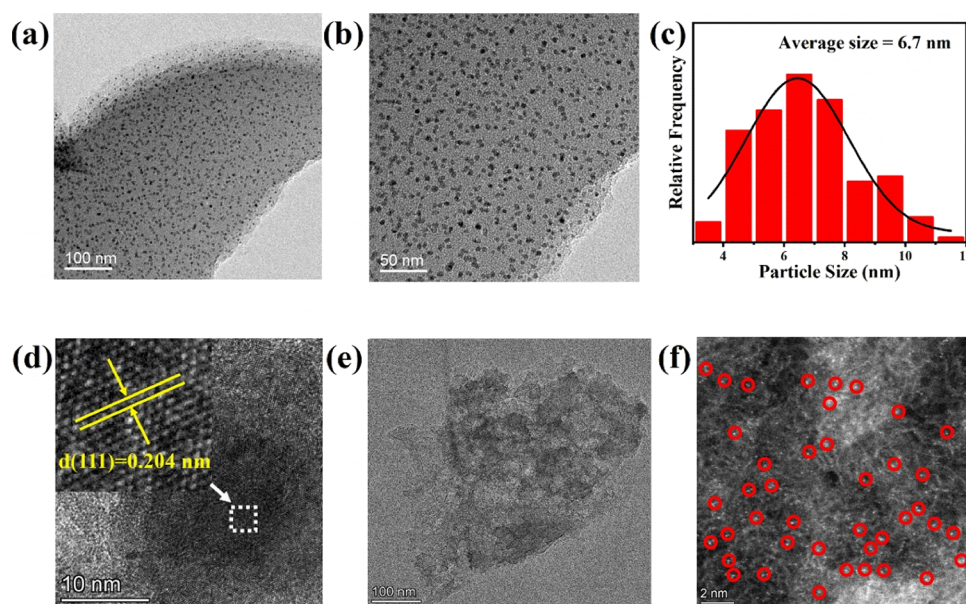


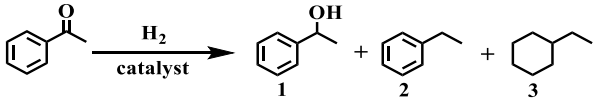
Figure 1. (a, b) TEM image, (c) particle distribution, and (d) HR-TEM images of Co@NC-600. (e) TEM and (f) AC-HAADF-STEM images of Co@NC-600-AT.

metallic cobalt (PDF#15-0806), respectively, while these peaks were not present in the XRD patterns of Co@NC-500.

TEM images revealed that Co nanoparticles with an average size of 6.7 nm were homogeneously distributed on the entire images of Co@NC-600 without significant aggregation (Figure 1a–c). Furthermore, the lattice spacing of 0.204 nm was measured in the high-resolution TEM (HR-TEM) image of Co@NC-600, assigned to the (111) crystalline plane of metallic Co nanoparticles (Figure 1d).²⁸ By increasing the pyrolysis temperature to 700 °C, cobalt nanoparticles in Co@NC-700 grew into larger size with an average size of 10.3 nm, and some aggregations were also observed (Figure S2). No cobalt nanoparticles or clusters were observed in the TEM image of Co@NC-500 (Figure S2), in accordance with the XRD results. However, a thick carbon layer was observed in the TEM image of Co@NC-500 (Figure S2). The EDS mapping displayed that Co, N, and C were distributed evenly in Co@NC-600 (Figure S3). In particular, the response signal of the Co element was relatively weak and extremely discrete, which indicated that Co atoms were highly dispersed on the catalyst surface. XPS was performed to probe the valence states of the surface elements. The N 1s XPS spectra of the Co@NC-T catalysts could be fitted into five peaks (Figure S4), corresponding to five different types of N as follows:²⁹ pyridinic N (398.5–398.7 eV), pyrrolic N (400.5–400.6 eV), Co–N_x (399.2–399.6 eV), graphitic N (401.3–401.4 eV), and oxidized N (402.3–402.5 eV), of which pyridinic N and pyrrolic N were the major nitrogen species. On the contrary, the fitted N 1s XPS spectra of Co/NC-600 showed no interaction between Co and N because of the absence of Co–N_x species (Figure S5). The C 1s XPS spectra of the representative Co@NC-600 catalyst (Figure S6) fitted into four peaks, including C–C/C=C (284.8 eV), C–N (285.7 eV), C–O (286.6 eV), and N=C–N (289.4 eV), which are consistent with the fitted N 1s XPS spectra. The peak with the binding energy of 778.2 eV can be fitted in the Co 2p_{3/2} XPS spectra of Co@NC-600 and Co@NC-700 (Figure S7), which was assigned to metallic Co, while this was not the case for Co@NC-500 and Co@NC-600-AT. This implies that the

Co@NC-600-AT catalyst had no Co–Co bond after acid treatment. The absence of metallic Co nanoparticles in Co@NC-500 was due to the fact that the Co cations could not be reduced into metallic Co nanoparticles at 500 °C, in accordance with the above XRD and TEM results. By the way, the presence of Co³⁺ with the binding energy around 783.2 eV in the Co 2p_{3/2} XPS spectra of Co@NC-600 and Co@NC-700 was due to the surface oxidation of metallic Co nanoparticles during the storage in air (Figure S7). In addition, the peak corresponding to Co²⁺ configuration, with the center at 780.8 eV, was also observed in the fitted Co 2p_{3/2} XPS spectra of the Co@NC-600 and Co@NC-600-AT catalysts (Figure S7), which was attributed to Co–N_x. The presence of Co–N_x species revealed that there existed a strong electronic interaction between the nitrogen and Co atoms. The surface areas and pore volumes of the Co@NC-T catalysts were further investigated based on the N₂ adsorption/desorption isotherms (Figure S8 and Table S1). Co@NC-500 had a very low surface area of 16.39 m²·g^{−1} and a very low pore volume of 0.03 cm³·g^{−1}, in good accordance with its thick-layered structure, as observed in the TEM image (Figure S2). However, the surface area and pore volume of Co@NC-600 greatly increased to 419.10 and 0.49 cm³·g^{−1} with the characteristic isotherm curves for microporous and mesoporous structures. The great increase in the surface area and pore volume from Co@NC-500 to Co@NC-600 was due to the release of much more volatile gases at the higher pyrolysis temperature. By further increasing the pyrolysis temperature to 700 °C, the surface area of Co@NC-700 contentiously increased to 462.22 m²·g^{−1}.

3.2. Catalyst Screening. The catalytic performance of the as-prepared Co catalysts was first evaluated by the reduction of acetophenone as the model reaction (Table 1). To our surprise, Co@NC-600 and Co@NC-700 could simultaneously catalyze the hydrodeoxygenation of C=O bond and the hydrogenation of the aromatic ring at 150 °C and 10 bar H₂ (Table 1, entries 2 and 3). Co@NC-600 demonstrated the highest catalytic activity, affording a nearly quantitative yield of ethylcyclohexane after 8 h. Compared with Co@NC-600, the

Table 1. Catalytic Reduction of Acetophenone over Different Catalysts^a


entry	catalyst	conversion (%)	selectivity (%)		
			1	2	3
1	Co@NC-500	0	0	0	0
2	Co@NC-600	100	0	1	99
3	Co@NC-700	100	0	19	81
4	Co@NC-600-AT	0	0	0	0
5	Co/NC-600	100	0	>99	0
6 ^b	Co@NC-600	100	0	>99	0

^aReaction conditions: acetophenone (0.5 mmol), catalyst (40 mg), 150 °C, H₂ (10 bar), 8 h, cyclohexane (5 mL), 800 rpm. ^bKSCN (1 mmol) was used.

lower catalytic activity of Co@NC-700 should be due to the larger size of Co nanoparticles (6.7 vs 10.3 nm), as Co nanoparticles with a larger size provide fewer sites to activate H₂ molecules. The inactivity of Co@NC-500 was due to the absence of metallic Co nanoparticles, which have been widely accepted to activate H₂ molecules for reduction reactions (Table 1, entry 1). To further study the role of metallic Co

nanoparticles, Co@NC-600-AT was also prepared by the acid treatment of Co@NC-600 to remove metallic Co nanoparticles for comparison. As shown in Figure S9, the XRD patterns of Co@NC-600-AT showed no peaks of metallic Co nanoparticles. Meanwhile, TEM measurements also showed that there were no visible Co nanoparticles in the entire TEM image of Co@NC-600-AT (Figure 1e). Therefore, XRD and TEM results confirmed that Co nanoparticles were successfully removed from Co@NC-600 by the acid treatment. Also, there was no detection of Co²⁺ in the hot filtration solution after leaching the Co@NC-600-AT catalyst. As expected, Co@NC-600-AT delivered no conversion (Table 1, entry 4), which further confirmed the crucial role of metallic Co nanoparticles in the activation of H₂ molecules to start the reaction.

Compared with the hydrogenation of the aromatic ring, the hydrodeoxygenation of C=O bonds in aromatic ketones was much easier. In fact, the hydrodeoxygenation of C=O bonds in aromatic ketones was also reported over heterogeneous Co and Ni catalysts,^{30,31} while the hydrogenation of the aromatic ring was almost performed over noble metal catalysts.^{19,32} Thus, it comes to probe the reasons of the high activity of the as-prepared Co@NC-600 catalyst toward the hydrogenation of the aromatic ring. The Co/NC-600 catalyst was prepared by the first step of impregnation of Co(NO₃)₂ on the surface of nitrogen-doped carbon, followed by the reduction of the impregnated Co cations with H₂ at 600 °C. XRD (Figure S10)

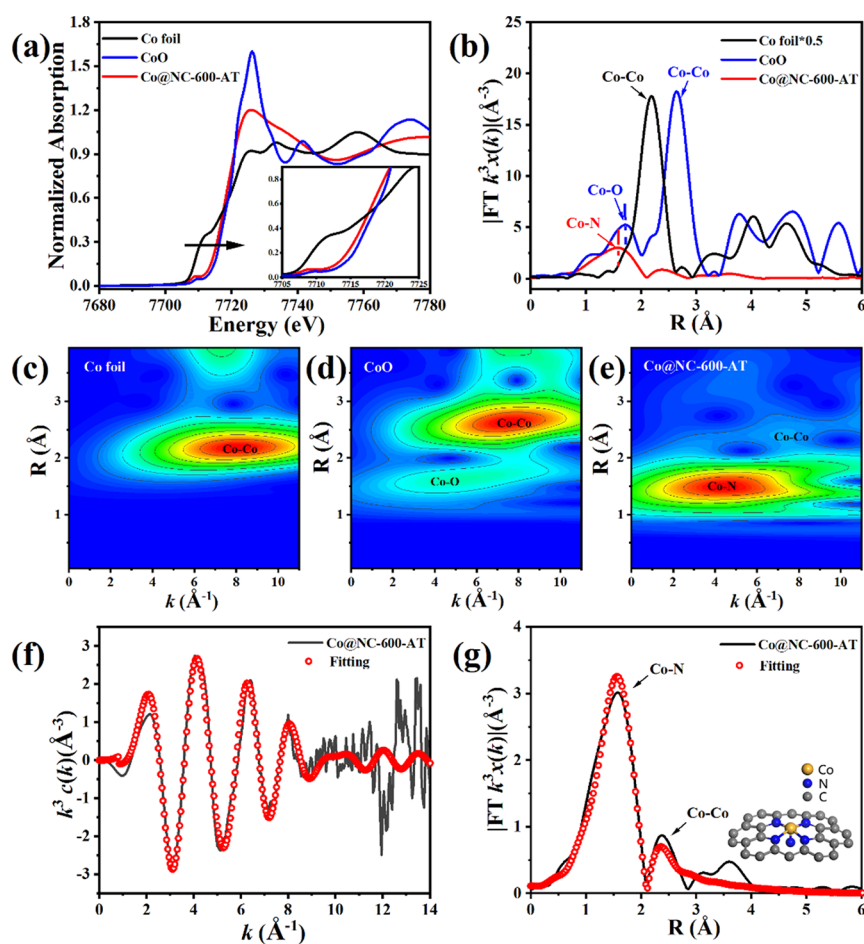


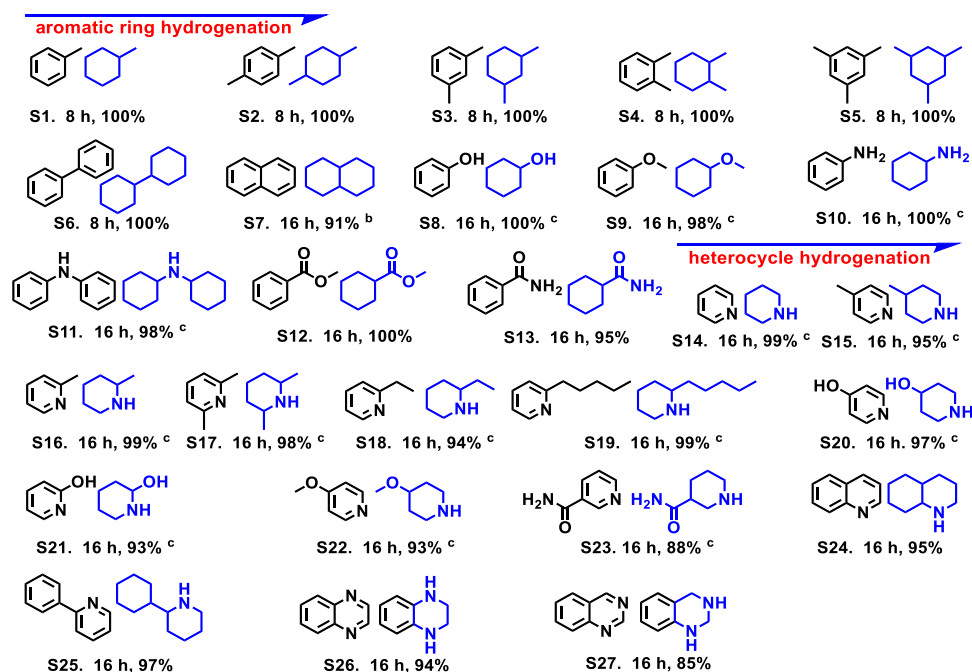
Figure 2. (a) Co K-edge XANES spectra of Co foil, CoO, and Co@NC-600-AT; (b) FT k^3 -weighted EXAFS spectra of Co foil, CoO, and Co@NC-600-AT; (c–e) wavelet-transformed k^3 -weighted EXAFS spectra of Co foil, CoO, and Co@NC-600-AT; (f) Co K-edge EXAFS fitting curves in k space; (g) Co K-edge EXAFS fitting curves in R space.

and TEM images (Figure S11) also revealed that the Co species in Co/NC-600 were the metallic Co nanoparticles. However, Co/NC-600 could only promote the hydrodeoxygenation of the C=O bond under the same conditions (Table 1, entry 5). In addition, the reaction using ethylbenzene as the starting material did not occur over Co/NC-600, further confirming that Co/NC-600 could only catalyze the hydrodeoxygenation of C=O bond in acetophenone. As both Co/NC-600 and Co@NC-600 had metallic Co nanoparticles, the catalytic activity of Co@NC-600 in the hydrogenation of the aromatic ring suggested that some other Co species should also be present in Co@NC-600 to promote the hydrogenation of the aromatic ring. Indeed, after the removal of Co nanoparticles from Co@NC-600 by acid treatment, the Co content in Co@NC-600-AT was determined to be 1.07 wt % by ICP-OES, while the Co content was below the detection limit for the Co/NC-600 sample by acid treatment. As many methods for the preparation of single Co atom catalysts were adopted the same procedure for the preparation of Co@NC-600-AT, the presence of Co species in Co@NC-600-AT should also be most likely presented as single Co atoms. The aberration-corrected high-angle annular dark-field scanning transmission electron microscopy (AC-HAADF-STEM) image indicates that single Co atoms with bright spots are clearly observed (Figure 1f), suggesting that Co@NC-600 was composed of metallic Co nanoparticles and single Co atoms. In previous literatures,^{18,19} Lewis acids were reported to play a crucial role in the activation of aromatic rings to assist metal nanoparticles to promote the hydrogenation of the aromatic ring. Thus, we believe that the single Co atoms in Co@NC-600 should also serve as the Lewis acid sites for the activation of aromatic ring and thus facilitate its hydrogenation over Co nanoparticles. Indeed, the acid amount of Co@NC-600-AT was determined to be 0.391 mmol·g⁻¹ by the NH₃-TPD method (Figure S12). KSCN has been extensively used as the poisoning reagent for single metal atom sites because of the strong affinity to single metal atoms.³³ Therefore, the poisoning experiment by KSCN was also performed. As expected, only ethylbenzene was produced in the presence of KSCN over the Co@NC-600 catalyst (Table 1, entry 6), further confirming the significant role of single Co atoms in the hydrogenation of the aromatic ring. In addition, other sulfur compounds (thiourea and thiophene) have been reported to be toxic to nanoparticles.³⁴ Therefore, in order to more fully study the synergistic effect of single Co atoms and Co nanoparticles on the catalyst, thiourea and thiophene were used to poison the Co nanoparticles on the catalyst Co@NC-600, and the corresponding additional experimental results are shown in Table S3. It could be seen from the table (entry 1) that the catalyst Co@NC-600 still had a high activity (conversion of acetophenone was 100%) after the single Co atom was poisoned, but the product stayed in the ethylbenzene stage. In particular, the catalyst poisoned by KSCN, with ethylbenzene as the starting reactant (entry 4), was almost inactive. This suggested that single Co atoms played a central role in ethylbenzene activation. After using thiourea or thiophene to poison Co nanoparticles (Table S3, entries 2, 3, 5, and 6), the hydrogenation reaction of ethylbenzene to ethylcyclohexane could still be carried out with impressive efficiency, which showed that the ethylbenzene activation process was hardly affected under the condition that single Co atoms were not poisoned. The decrease in the yield of ethylcyclohexane was most likely due to the decrease in the

dissociation rate of H₂ caused by the poisoning of Co nanoparticles.

EXAFS measurements at the Co K-edge were performed to investigate the chemical state and coordination environment of the single Co atoms in the Co@NC-600 catalyst by collecting data from Co@NC-600-AT. Figure 2a shows the XANES spectra of Co@NC-600-AT along with the standard Co foil and CoO references. Co@NC-600-AT displays a significantly different XANES profile in comparison with those from the corresponding references. The position of the absorption edge for Co@NC-600-AT is far away from that for Co foil but is close to that for CoO, suggesting that the valence state of the single Co atoms in Co@NC-600-AT was close to +2. The corresponding Fourier transforms (FTs) obtained from EXAFS showed that the main peak of Co@NC-600-AT at ≈1.58 Å was attributed to the Co–N bond, which is shorter than the Co–O peak at 1.70 Å of the standard CoO (Figure 2b). In contrast, no Co–Co peaks or other high-shell peaks were observed for Co@NC-600-AT. Additionally, the wavelet transforms (WTs) of Co K-edge EXAFS oscillations were also observed (Figure 2c–e). The contour plots of Co@NC-600-AT present only one intensity maximum at 4.40 Å⁻¹, corresponding to Co–N coordination, and no intensity maximum related to Co–Co coordination and Co–O coordination can be detected, compared with that of Co foil and CoO references. These results evidently suggest that the Co species in Co@NC-600-AT are atomically dispersed and coordinated by nitrogen atoms. Quantitative EXAFS fittings in *k* space and *R* space were then conducted to extract the structural parameters and obtain the precise coordination configuration of Co atom for Co@NC-600-AT (Figure 2f,g). The best-fitting analysis reveal that the coordination number of the central Co atom is about 5, and the mean bond length of Co@NC-600-AT is 2.04 Å (Table S4). Figure 2g also shows the presence of a small proportion of Co–Co bonds in Co@NC-600-AT after acid treatment, again confirming the coexistence of single Co atoms and Co nanoparticles. Therefore, the Co atomic structure model can be described, as shown in the inset of Figure 2g, in which each single Co atom is coordinated by four nitrogen atoms in the plane and one nitrogen atom in the axial position.

Moreover, the reaction solvents showed a great influence on the reduction of acetophenone over the Co@NC-600 catalyst (Table S5). Cyclohexane and hexane emerged as good solvents to produce ethylcyclohexane as the sole or main product, while the reaction in oxygen-containing solvents including water, polar, and nonpolar solvents produced ethylbenzene with selectivity >97%. The oxygen-containing solvents should have a strong affinity to the single Co atoms via acid–base interaction to block the single Co atom sites for the activation of the aromatic ring, similar to the poisoning of single Co atoms by KSCN. To further confirm the above statements, some control experiments on the hydrogenation of ethylbenzene were also performed (Table S6). Indeed, the hydrogenation of ethylbenzene almost stopped in ethanol, while quantitative conversion was observed in cyclohexane. More interestingly, the conversion of ethylbenzene greatly decreased from 100% in cyclohexane to 7% in the presence of 2% volume ethanol in cyclohexane, while *tert*-amyl alcohol with 2% volume in cyclohexane showed no significant influence on the hydrogenation of ethylbenzene. The huge difference was due to the great difference in the steric hindrance between ethanol and *tert*-amyl alcohol. Ethanol

Table 2. Selective Hydrogenation of Aromatic Rings over the Co@NC-600 Catalyst^a

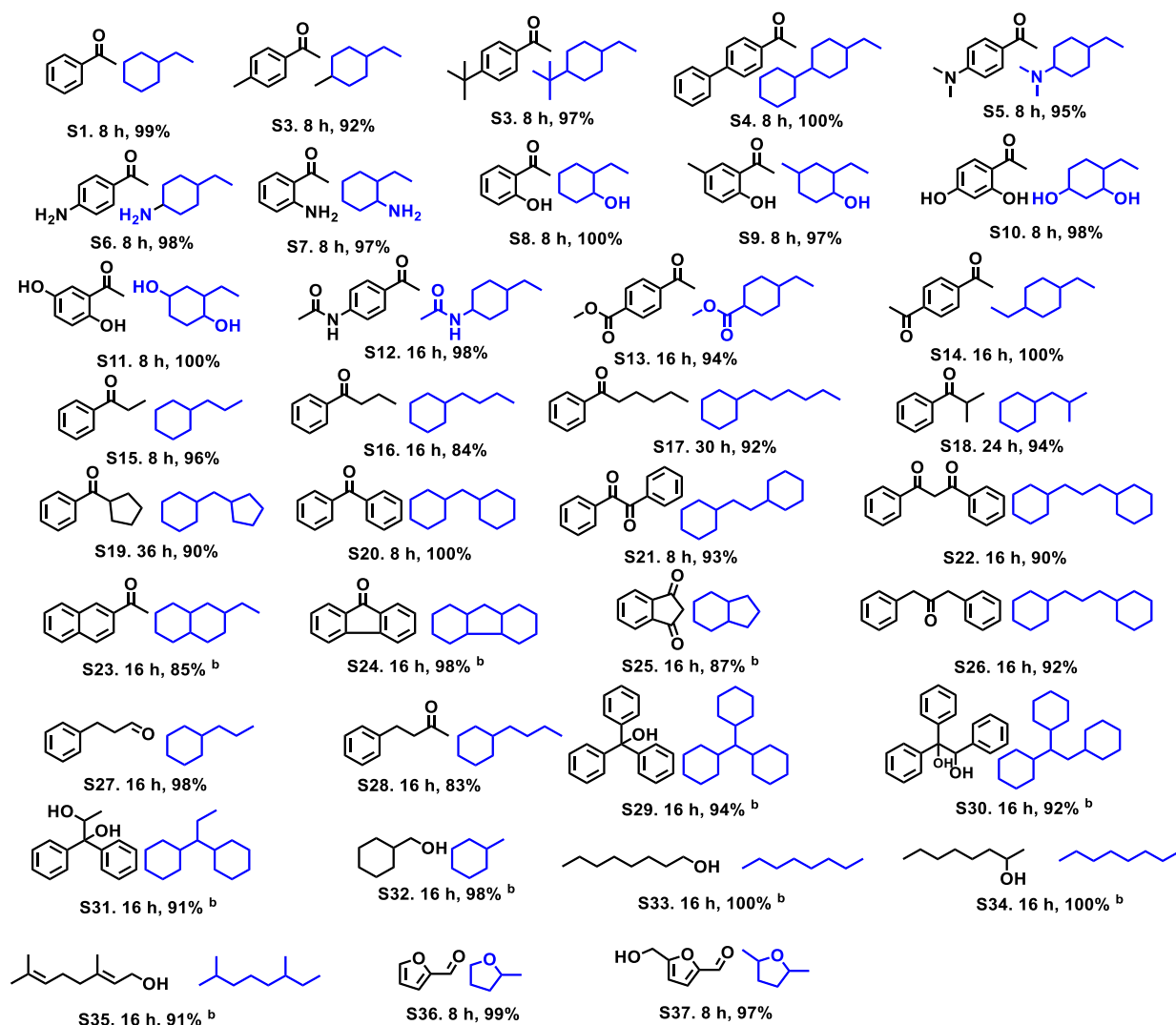
^aReaction conditions: substrate (0.5 mmol), the Co@NC-600 catalyst (40 mg), 150 °C, H₂ (10 bar), cyclohexane (5 mL), and 800 rpm. ^b190 °C. ^c130 °C.

could combine with the single Co atoms freely, while that was not the case for *tert*-amyl alcohol with a large steric hindrance.

Besides the reaction solvents, the reaction temperature also showed a great influence on the product distribution (Figure S13). 1-Phenylethanol was the sole product at 70 °C, while ethylbenzene was the major product at 90–110 °C. As far as the hydrodeoxygenation of 1-phenylethanol into ethylbenzene is concerned, two reaction pathways have been generally reported. One way is the dehydration–hydrogenation pathway (Scheme S1), which involves the first step of the dehydration of 1-phenylethanol into styrene, followed by the hydrogenation of styrene into ethylbenzene. The other way is the direct hydrogenolysis process. Generally, the catalysts with Lewis acid sites tend to promote the dehydration of 1-phenylethanol into styrene.^{5,35} This suggests that the hydrodeoxygenation of 1-phenylethanol into ethylbenzene proceeded via styrene as the intermediate. The final step of the hydrogenation of the aromatic ring in ethylbenzene into ethylcyclohexane started at 130 °C and greatly accelerated at 150 °C. After 8 h, acetophenone was quantitatively converted into ethylcyclohexane over the Co@NC-600 catalyst at 150 °C and 10 bar H₂. Kinetic experiments of the hydrogenation of acetophenone into 1-phenylethanol, the hydrodeoxygenation of 1-phenylethanol into ethylbenzene, and the hydrogenation of ethylbenzene into ethylcyclohexane were studied. These kinetic experiments were performed under 30 bar H₂, and thus the H₂ concentration in the reaction solvent could be considered to be constant. Thus, the reactions should most likely be pseudo-first-order reactions. According to the Arrhenius equation, ln *k* versus 1/*T* was plotted in Figure S14, where *k* is the reaction rate constant, and the calculated activation energies (*E*_a) were determined to be 83.06, 97.09, and 110.17 kJ·mol⁻¹ for the hydrogenation of acetophenone into 1-phenylethanol, the hydrodeoxygenation of 1-phenylethanol into ethylbenzene, and the hydrogenation of ethylbenzene into ethylcyclohexane,

respectively. These results clearly revealed that the consecutive steps became much more difficult and that the hydrogenation of the aromatic ring was the rate-determining step over the Co@NC-600 catalyst. Unlike the reaction temperature and reaction solvents, the H₂ pressure showed no significant influence on the reduction of acetophenone (Table S7). This is most probably because the H₂ pressure is not the decisive factor affecting this reaction. From the DFT calculation in Figure S17, it can be seen that the dissociation energy barrier of H₂ on Co nanoparticles is extremely low, only 0.27 eV. This indicates that the catalyst easily dissociates H₂, which will bring sufficient H spillover on the surface of the catalyst even under low H₂ pressure. It will lead to the subsequent continued increase of the H₂ pressure to have little effect on the concentration of dissociated H on the catalyst surface, thus not having a significant influence on the hydrodeoxygenation of acetophenone. In addition, Co@NC-600 demonstrated a high stability without the significant loss of its catalytic activity and product selectivity (Figure S15).

3.3. Substrate Scope. The catalytic hydrogenation of the aromatic ring as well as heteroaromatic rings remains one of the important organic transformations to access liquid fuels, drug discovery, and material sciences.^{36–41} Co@NC-600 was first used for the hydrogenation of aromatic rings as well as heteroaromatic rings in different types of substrates. As shown in Table 2, different kinds of aromatic hydrocarbons (S1–S7) were successfully hydrogenated into the corresponding cyclic hexane derivatives at 150 °C and 10 bar H₂, demonstrating their good potential in the production of high-energy-density liquid fuels. Co@NC-600 was even active for 1,3,5-trimethylbenzene (S5) with a large steric hindrance, and naphthalene (S7) with an inert fused ring, but the full hydrogenation of the fused ring in naphthalene required a high reaction temperature of 190 °C. In addition, two aromatic

Table 3. Catalytic Hydrodeoxygenation and Ring Hydrogenation over Co@NC-600^a

^aReaction conditions: substrate (0.5 mmol), the Co@NC-600 catalyst (40 mg), 150 °C, H₂ (10 bar), cyclohexane (5 mL), and 800 rpm. ^b190 °C.

rings in biphenyl (S6) could be simultaneously hydrogenated over Co@NC-600 at 150 °C.

Besides aromatic hydrocarbons, Co@NC-600 was also effective for the selective hydrogenation of aromatic rings in these substrates bearing functional groups such as hydroxyl, ammonia, ester, ether, and amides (S8–S13). Interestingly, substrates with electron-donating substituted groups (S8–S11) were more active than those with electron-withdrawing substituted groups (S12 and S13), suggesting that aromatic rings with higher electron density are more active. Furthermore, Co@NC-600 was also active for the hydrogenation of N-heteroaromatic rings including pyridine, quinoline, quinoxaline, and quinazoline to give rise to the saturated heterocyclic products (S14–S27). Generally, it is difficult to carry out the hydrogenation of heteroaromatic substrates, as these substrates can poison the metal sites due to the strong interaction between them. In contrast, the strong interaction of the single Co atoms in Co@NC-600 with the heteroatoms in the heteroaromatic ring (Lewis acid–Lewis base interaction) could activate the heteroaromatic rings more efficiently, and thus the hydrogenation of the heteroaromatic rings could be performed smoothly over Co@NC-600. The simultaneous

hydrogenation of the aromatic ring as well as the heteroaromatic ring was observed for S24 and S25, while only hydrogenation of the N-heterocyclic ring was observed for quinoxaline (S26) and quinazoline (S27).

After the success in the hydrogenation of the aromatic ring, the scope of the simultaneous hydrogenation of the aromatic ring and the hydrodeoxygenation of C=O/C–OH bonds was explored over the Co@NC-600 catalyst (Table 3). First, the reduction of aryl-methyl ketones was studied (S1–S13). Again, it was noted that the aryl-methyl ketones with electron-donating substituted groups (S1–S11) were more active than those with the electron-withdrawing substituted groups (S12 and S13), where the latter required a longer reaction time to get high yields. Besides the hydrodeoxygenation of ketone groups and the hydrogenation of the aromatic ring, these substituted groups in the aromatic ring were also well tolerant under the reaction conditions, which are of great importance in organic transformations. 1,4-Diacetylbiphenyl (S14) with two methyl ketone groups were quantitatively reduced to saturated 1,4-diethyl-cyclohexane after 16 h at 150 °C and 10 bar H₂. Besides aryl-methyl ketones, aryl-alkyl (cyclic) ketones (S15–S19), aryl-aryl ketone (S20), and aryl-aryl diketones (S21–

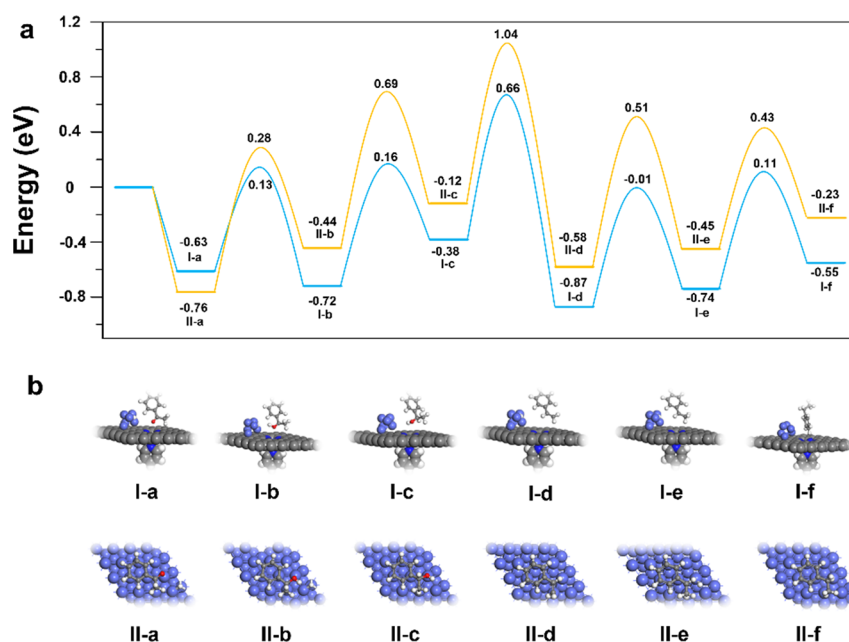


Figure 3. (a) Energy profiles of acetophenone hydrogenation to ethylbenzene on the catalyst with single Co atom and Co nanoparticles (blue line), as well as the catalyst only with metallic Co nanoparticles (yellow line). (b) Main structures of the reaction molecule, intermediates, and the product on the two catalysts.

S22) were also successfully reduced to the corresponding saturated compounds. Compared with aryl-methyl ketones, the steric hindrance of the alkyl or cyclic groups in aryl-alkyl (cyclic) ketones was clearly observed (S1 vs S15–S19). More obviously, the fuse-ring ketones (S23 and S24) as well as the cyclic diketone (S25) with the large steric hindrance required the high reaction temperature of 190 °C to get the saturated products with high yields. Besides the aromatic ketones, Co@NC-600 was also effective for the simultaneous hydrogenation of the aromatic ring and the hydrodeoxygenation of isolated C=O bonds (S26–S28) at 150 °C and 10 bar H₂. The aromatic alcohols/diols with large steric hindrance (S29–S31) and aliphatic substrates (S32–S35) were less active, which were reacted at a higher reaction temperature of 190 °C to get high yields of the saturated hydrocarbons. Furfural and 5-hydroxymethylfurfural (HMF) represent two of the most important biomass-based platform chemicals from the dehydration of carbohydrates.^{42,43} The catalytic reduction of furfural and HMF into tetrahydrofuran derivatives is a highly attractive route to access renewable fuels as well as the organic solvents, but it remains a great challenge due to the serious side reactions such as the formation of humins and the inert furan ring.⁴⁴ For example, the Ru/C-based catalytic system could only give rise to 76% yield of 2,5-dimethyltetrahydrofuran (DMTHF) from HMF at 180 °C and 50 bar H₂ in 1,4-dioxane.⁴⁴ To our great pleasure, the Co@NC-600 catalyst could successfully promote the hydrogenation of the furan ring and the hydrodeoxygenation of C=O/C–OH bonds in furfural (S36) and HMF (S37) with nearly quantitative yields of 2-methyltetrahydrofuran and DMTHF under much more mild conditions (150 °C and 10 bar H₂).

3.4. Mechanism Study. According to the characterization of Co@NC-600 and the controlled experiments, the excellent catalytic performance on the hydrodeoxygenation of C=O/C–OH bonds and hydrogenation of the aromatic ring over the Co@NC-600 catalyst was due to the synergistic roles of single Co atoms and metallic Co nanoparticles, where the single Co

atoms served as the Lewis acid sites in the activation of aromatic rings, and the Co nanoparticles served a role in the activation of H₂ molecules to generate the active hydrogen species. In this section, DFT calculation was resorted to further study the reaction mechanism of the hydrodeoxygenation of the C=O bond and the hydrogenation of the aromatic ring in acetophenone. First, the DFT model was constructed according to the characterized structure of the Co@NC-600 catalyst, which was composed of single Co atoms bearing Co–N₅ motifs in the carbon layer and the supported Co nanoparticles on the surface of the carbon layer (Figure S16). The adsorption energy of H₂ and the energy barriers for the heterolytic cleavage of H₂ molecules to generate the active H species on the surface of Co nanoparticles were calculated to be –0.16 and 0.27 eV, respectively (Figure S17). As far as the hydrogenation of acetophenone into 1-phenylethanol is concerned, the H atom on the surface of Co nanoparticles can first be added to the O atom in the C=O bond or the C atom in the C=O bond. DFT calculations revealed that the addition of the first H atom to the O atom in the C=O bond was preferable with the lower energy barrier (0.76 vs 1.11 eV, Figures 3 and S18). After the addition of the first H atom to the O atom in the C=O bond to generate the reactive I-b species, the addition of the second H atom to the C atom gives rise to the 1-phenylethanol intermediate I-c with the energy barrier of 0.88 eV (Figure 3). Compared with the reaction over the catalyst with metallic Co nanoparticles and single Co atoms, the energy barriers of the addition of two H atoms to the O atom and C atom in acetophenone were calculated to be 1.04 and 1.13 eV over the surface of metallic Co nanoparticles without the assistance of single Co atoms, respectively (Figure 3). These data revealed that the single Co atoms could lower the energy barriers of the hydrogenation of C=O bond into C–OH bond over metallic Co nanoparticles, where the single Co atoms should serve as the Lewis acid sites to activate the C=O bond. The optimized structure showed that acetophenone was adsorbed on single Co atoms through the carbonyl-

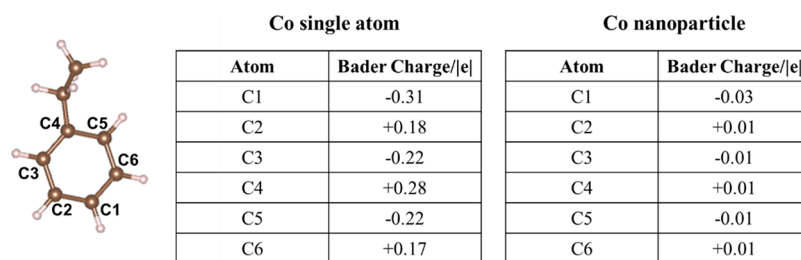


Figure 4. Bader charge analysis of ethylbenzene adsorbed on a single Co atom and Co nanoparticles.

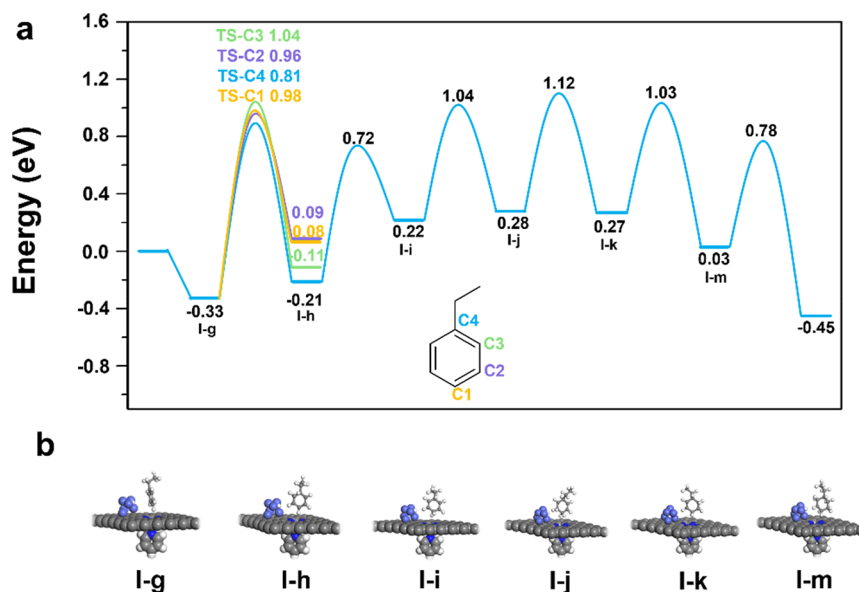


Figure 5. (a) Energy profiles of the hydrogenation of ethylbenzene to ethylcyclohexane over the catalyst with metallic Co nanoparticles and the single Co atoms. (b) Main structures of the reaction molecule, intermediates, and the product on the catalyst.

terminal O atom. It would lead to the transfer of electrons from O to Co. The electron density on C=O decreased, and the C atom would be prone to hydrogenation reaction. Therefore, the single Co atom acted as a Lewis acid in this activation process.

As discussed above, the following step is the dehydration of 1-phenylethanol into styrene, which should proceed via the synergistic cleavage of C–H bond and C–OH bond in 1-phenylethanol to release one water molecule. DFT calculations also revealed that single Co atoms serving as the Lewis acid sites also lowered the energy barrier of the dehydrogenation of 1-phenylethanol into styrene from 1.16 to 1.04 eV (Figure 3). Then, the step-by-step addition of two H atoms to the C=C bond in styrene generates the ethylbenzene intermediate. The addition of the first H atom to the terminal carbon in styrene to generate I-e active species over the metallic Co and single Co atom or II-e active species over the metallic Co without the single Co atom was much more difficult than the addition of the second H atom to I-e or II-e active species to generate ethylbenzene. In addition, it was found that the presence of single Co atom sites in the catalyst also showed a positive effect on the addition of the first H atom, lowering the energy barrier from 1.09 to 0.86 eV. In addition, DFT calculations also revealed that the dehydration of 1-phenylethanol into styrene was the rate-determining step during the hydrodeoxygenation of the C=O bond in acetophenone, in good accordance with the experimental results.

Then, particular interest was paid to the significant role of single Co atoms with the assistance of metallic Co nanoparticles toward the hydrogenation of the aromatic ring. According to the references¹⁹ and the experimental data, the single Co atoms should serve as the Lewis acid sites to combine with the electron-rich aromatic ring, and thus the electron density of each carbon should be changed, resulting in the activation of the aromatic ring. The single Co atom should combine with the C1 atom in the aromatic ring at the para-position of the ethyl group in ethylbenzene (Figure 4), due to the weakest steric hindrance. First, the electron density of each carbon in the aromatic ring after the activation of ethylbenzene by a single Co atom site was calculated. For comparison, the electron density of each carbon in the aromatic ring without the activation by the single Co atom catalyst was also calculated. As shown in Figure 4, the electron density of each carbon in the aromatic ring was very close to each other on the surface of metallic Co nanoparticles. However, the electron density of each carbon greatly changed after the activation by a single Co atom (Figure 4), and thus the aromatic ring in ethylbenzene was more active to be hydrogenated. For example, the electron density of C1 atom on the surface of Co nanoparticles was only -0.03 eV, while it was calculated to be -0.31 eV after the activation by a single Co atom. Particularly, the calculated data were also consistent with the experimental rule of chemistry. The direct interaction of a single Co atom with the C1 atom resulted in the enrichment of the electron from the aromatic ring to the C1

atom; thus, the electron density of C1 atom was the most negative. Meanwhile, the electron density of C4 atom had a positive charge of +0.28 eV, which could be stabilized by the ethyl group. Therefore, the addition of one H₂ molecule (H⁺–H[–]) should first add a C1 atom and a C4 atom to generate the 3-ethyl-1,4-cyclohexadiene intermediate. DFT calculations (Figure 5) also revealed that the energy barrier of the addition of the first H atom to the C4 atom was lower (1.14 eV) than those to the C1 atom (1.31 eV), C2 atom (1.29 eV), and C3 atom (1.37 eV). Therefore, the addition of the first H atom to the aromatic ring should be added to the C4 atom, according to the above analysis, which required the lowest energy barrier for all the steps. After the addition of the first H atom to the C4 atom, the addition of the second H atom to the C1 atom to generate the 3-ethyl-1,4-cyclohexadiene intermediate requires a low energy barrier of 0.93 eV (Figure 5). Then, the consecutive addition of four H atoms from two H₂ molecules into the two C=C bonds in 3-ethyl-1,4-cyclohexadiene proceeded smoothly, as the calculated energy barriers (0.75–0.84 eV) of these steps were all lower than those of the addition of the first two H atoms to the C4 atom and C1 atom (Figure 5). In addition, the hydrogenation of the aromatic ring without activation by the single Co atom was also calculated. The addition of the first H atom to the C1, C2, C3, and C4 atoms in ethylbenzene was also calculated over metallic Co nanoparticles (Figure S19), and the energy barriers were very high up to 2.13, 1.98, 2.08, and 1.96 eV with the addition of one H atom to C1, C2, C3, and C4 atoms, respectively. These data clearly reveal that the hydrogenation of the aromatic ring became much easier after the activation by a single Co atom.

4. CONCLUSIONS

In summary, we have developed a novel heterogeneous non-noble metal catalytic method for the simultaneous hydrodeoxygenation of C=O/C–OH bonds and hydrogenation of the aromatic ring with the Co@NC-T catalyst. The excellent catalytic performance of Co@NC-600 was due to the synergistic roles of single Co atoms and metallic Co nanoparticles. Co nanoparticles served a role in the activation of H₂ molecule to generate the active hydrogen species for the hydrodeoxygenation of C=O/C–OH bonds and hydrogenation of the aromatic ring. The controlled experiments and DFT calculations revealed that the single Co atom in the Co@NC-600 catalyst could serve as the Lewis acid site to promote the hydrodeoxygenation of C=O/C–OH bonds as well as the hydrogenation of the aromatic ring. Kinetic studies as well as DFT calculations revealed that the hydrogenation of the aromatic ring was much more difficult with a higher activation energy than the hydrodeoxygenation of C=O/C–OH bonds. DFT calculations revealed that the single Co atom could greatly disturb the electron density of each carbon in the aromatic ring by the electronic interaction with the aromatic ring; thus, the activated aromatic ring was much easier to be hydrogenated. Compared with the reaction on the metallic Co nanoparticles, the activation by the single Co atom greatly lowered the energy barriers of the hydrogenation of the inert aromatic ring from 1.96 to 1.14 eV. The utility of the catalyst opens new avenues for the synthesis of saturated cyclohexane derivatives and heterocyclic compounds, demonstrating a great potential in the fields of energy storage as well as the production of high-value chemicals with specific structures.

■ ASSOCIATED CONTENT

SI Supporting Information

The Supporting Information is available free of charge at <https://pubs.acs.org/doi/10.1021/acs.jpcc.3c02352>.

Experimental section including materials and characterization details, analytical methods, and computational details; XRD patterns, TEM images, and particle size distribution; TEM mapping of Co@NC-600; XPS spectra, N₂ adsorption–desorption isotherms, NH₃-TPD profile, and results of the hydrogenation and hydrodeoxygenation of acetophenone at different reaction temperatures; reaction routes of the transformation of acetophenone into ethylcyclohexane; kinetic studies; recyclability of Co@NC-600; constructed models of the Co@NC-600 catalyst, energy profile of H₂ activation on Co nanoparticles; energy profile of acetophenone hydrogenation on single Co atoms; energy profile of the first step for ethylbenzene hydrogenation on Co nanoparticles; textural parameters and element analysis of the Co@NC-T catalysts; effect of poisoning reagent over Co@NC-600; EXAFS fitting parameters at the Co K-edge; effect of the solvents on the reduction of acetophenone and on the hydrogenation of ethylbenzene; effect of hydrogen pressure on the reduction of acetophenone; and MS spectra for all compounds (PDF)

■ AUTHOR INFORMATION

Corresponding Authors

Duan-Jian Tao – National Engineering Research Center for Carbohydrate Synthesis, Key Laboratory of Fluorine and Silicon for Energy Materials and Chemistry of Ministry of Education, College of Chemistry and Chemical Engineering, Jiangxi Normal University, Nanchang 330022, P.R. China; orcid.org/0000-0002-8835-0341; Email: djtao@jxnu.edu.cn

Zehui Zhang – Key Laboratory of Catalysis and Materials Sciences of the Ministry of Education, South-Central Minzu University, Wuhan 430074, P.R. China; orcid.org/0000-0003-1711-2191; Email: zehuizh@mail.uustc.edu.cn

Authors

Song Han – National Engineering Research Center for Carbohydrate Synthesis, Key Laboratory of Fluorine and Silicon for Energy Materials and Chemistry of Ministry of Education, College of Chemistry and Chemical Engineering, Jiangxi Normal University, Nanchang 330022, P.R. China

Ruijie Gao – College of Materials and Chemistry, China University of Geosciences, Wuhan 430074, P.R. China

Ming-Shuai Sun – National Engineering Research Center for Carbohydrate Synthesis, Key Laboratory of Fluorine and Silicon for Energy Materials and Chemistry of Ministry of Education, College of Chemistry and Chemical Engineering, Jiangxi Normal University, Nanchang 330022, P.R. China; orcid.org/0000-0002-5126-4159

Yan Zhou – National Engineering Research Center for Carbohydrate Synthesis, Key Laboratory of Fluorine and Silicon for Energy Materials and Chemistry of Ministry of Education, College of Chemistry and Chemical Engineering, Jiangxi Normal University, Nanchang 330022, P.R. China; orcid.org/0000-0003-0108-5061

Wen-Ting Chen – National Engineering Research Center for Carbohydrate Synthesis, Key Laboratory of Fluorine and Silicon for Energy Materials and Chemistry of Ministry of Education, College of Chemistry and Chemical Engineering, Jiangxi Normal University, Nanchang 330022, P.R. China

Xixi Liu – Key Laboratory of Catalysis and Materials Sciences of the Ministry of Education, South-Central Minzu University, Wuhan 430074, P.R. China

Jingzhong Qin – Key Laboratory of Catalysis and Materials Sciences of the Ministry of Education, South-Central Minzu University, Wuhan 430074, P.R. China

Complete contact information is available at:
<https://pubs.acs.org/10.1021/acs.jpcc.3c02352>

Author Contributions

[†]S.H and R.G. contributed equally. D.T. and Z.Z. conceived the initial idea and experimental design. S.H. carried out and analyzed the experiments. R.G. carried out the DFT calculations. M.S., Y.Z., W.C., X.L., and J.Q. contributed to the data analyses. All authors discussed the results and commented on the manuscript. S.H., R.G., D.T., and Z.Z. wrote the paper with help from all authors.

Notes

The authors declare no competing financial interest.

ACKNOWLEDGMENTS

We thank the Key Lab of Fluorine and Silicon for Energy Materials and Chemistry of Ministry of Education, Jiangxi Normal University (KFSEMC-202209), and Hubei Provincial Natural Science Foundation of China (2020CFA096) for the financial support.

REFERENCES

- (1) Kumar, A.; Daw, P.; Milstein, D. Homogeneous Catalysis for Sustainable Energy: Hydrogen and Methanol Economies, Fuels from Biomass, and Related Topics. *Chem. Rev.* **2022**, *122*, 385–441.
- (2) Li, J.; Huang, H.; Xue, W.; Sun, K.; Song, X.; Wu, C.; Nie, L.; Li, Y.; Liu, C.; Pan, Y.; et al. Self-Adaptive Dual-Metal-Site Pairs in Metal–Organic Frameworks for Selective CO₂ Photoreduction to CH₄. *Nat. Catal.* **2021**, *4*, 719–729.
- (3) Zhang, L.; Zhou, M.; Wang, A.; Zhang, T. Selective Hydrogenation over Supported Metal Catalysts: from Nanoparticles to Single Atoms. *Chem. Rev.* **2020**, *120*, 683–733.
- (4) Deng, Q.; Hou, X.; Zhong, Y.; Zhu, J.; Wang, J.; Cai, J.; Zeng, Z.; Zou, J. J.; Deng, S.; Yoskamtor, T.; et al. 2D MOF with Compact Catalytic Sites for the One-Pot Synthesis of 2,5-Dimethylfuran from Saccharides via Tandem Catalysis. *Angew. Chem., Int. Ed.* **2022**, *61*, No. e202205453.
- (5) Schwob, T.; Kunnas, P.; de Jonge, N.; Papp, C.; Steinrück, H. P.; Kempe, R. General and Selective Deoxygenation by Hydrogen Using a Reusable Earth-Abundant Metal Catalyst. *Sci. Adv.* **2019**, *5*, No. eaav3680.
- (6) Rahimi, A.; Ulbrich, A.; Coon, J. J.; Stahl, S. S. Formic-Acid-Induced Depolymerization of Oxidized Lignin to Aromatics. *Nature* **2014**, *515*, 249–252.
- (7) Xiang, S.; Dong, L.; Wang, Z. Q.; Han, X.; Daemen, L. L.; Li, J.; Cheng, Y.; Guo, Y.; Liu, X.; Hu, Y.; et al. A Unique Co@CoO Catalyst for Hydrogenolysis of Biomass-Derived 5-Hydroxymethylfurfural to 2,5-Dimethylfuran. *Nat. Commun.* **2022**, *13*, 3657.
- (8) Tang, X.; Ding, W.; Li, H. Improved Hydrodeoxygenation of Bio-Oil Model Compounds with Polymethylhydrosiloxane by Brønsted Acidic Zeolites. *Fuel* **2021**, *290*, No. 119883.
- (9) Offner-Marko, L.; Bordet, A.; Moos, G.; Tricard, S.; Rengshausen, S.; Chaudret, B.; Luska, K. L.; Leitner, W. Bimetallic Nanoparticles in Supported Ionic Liquid Phases as Multifunctional

Catalysts for the Selective Hydrodeoxygenation of Aromatic Substrates. *Angew. Chem., Int. Ed.* **2018**, *57*, 12721–12726.

(10) Bordet, A.; Leitner, W. Metal Nanoparticles Immobilized on Molecularly Modified Surfaces: Versatile Catalytic Systems for Controlled Hydrogenation and Hydrogenolysis. *Acc. Chem. Res.* **2021**, *54*, 2144–2157.

(11) Ning, H.; Chen, Y.; Wang, Z.; Mao, S.; Chen, Z.; Gong, Y.; Wang, Y. Selective Upgrading of Biomass-Derived Benzylic Ketones by (Formic Acid)–Pd/HPC–NH₂ System with High Efficiency under Ambient Conditions. *Chem* **2021**, *7*, 3069–3084.

(12) Zong, R.; Li, H.; Ding, W.; Huang, H. Highly Dispersed Pd on Zeolite/Carbon Nanocomposites for Selective Hydrodeoxygenation of Biomass-derived Molecules Under Mild Conditions. *ACS Sustainable Chem. Eng.* **2021**, *9*, 9891–9902.

(13) Song, Y.; Feng, X.; Chen, J. S.; Brzezinski, C.; Xu, Z.; Lin, W. Multistep Engineering of Synergistic Catalysts in a Metal–Organic Framework for Tandem C–O Bond Cleavage. *J. Am. Chem. Soc.* **2020**, *142*, 4872–4882.

(14) Li, H.; Gao, Z.; Lei, L.; Liu, H.; Han, J.; Hong, F.; Luo, N.; Wang, F. Photocatalytic Transfer Hydrogenolysis of Aromatic Ketones Using Alcohols. *Green Chem.* **2020**, *22*, 3802–3808.

(15) Rakers, L.; Martínez-Prieto, L. M.; López-Vinasco, A. M.; Philippot, K.; van Leeuwen, P. W. N. M.; Chaudret, B.; Glorius, F. Ruthenium Nanoparticles Ligated by Cholesterol-Derived NHCs and Their Application in the Hydrogenation of Arenes. *Chem. Commun.* **2018**, *54*, 7070–7073.

(16) Kumar, A.; Goyal, V.; Sarki, N.; Singh, B.; Ray, A.; Bhaskar, T.; Bordoloi, A.; Narani, A.; Natte, K. Biocarbon Supported Nanoscale Ruthenium Oxide-Based Catalyst for Clean Hydrogenation of Arenes and Heteroarenes. *ACS Sustainable Chem. Eng.* **2020**, *8*, 15740–15754.

(17) Martin, J.; Knupfer, C.; Eysel, J.; Farber, C.; Grams, S.; Langer, J.; Thum, K.; Wiesinger, M.; Harder, S. Highly Active Superbulky Alkaline Earth Metal Amide Catalysts for Hydrogenation of Challenging Alkenes and Aromatic Rings. *Angew. Chem., Int. Ed. Engl.* **2020**, *59*, 9102–9112.

(18) Liu, H.; Jiang, T.; Han, B.; Liang, S.; Zhou, Y. Selective Phenol Hydrogenation to Cyclohexanone over a Dual Supported Pd–Lewis Acid Catalyst. *Science* **2009**, *326*, 1250–1252.

(19) Miyamura, H.; Kobayashi, S. Reaction Rate Acceleration of Cooperative Catalytic Systems: Metal Nanoparticles and Lewis Acids in Arene Hydrogenation. *Angew. Chem., Int. Ed.* **2022**, *61*, No. e202201203.

(20) Zhou, P.; Jiang, L.; Wang, F.; Deng, K.; Lv, K.; Zhang, Z. High Performance of a Cobalt–Nitrogen Complex for the Reduction and Reductive Coupling of Nitro Compounds into Amines and Their Derivatives. *Sci. Adv.* **2017**, *3*, No. e1601945.

(21) Xie, C.; Lin, L.; Huang, L.; Wang, Z.; Jiang, Z.; Zhang, Z.; Han, B. Zn–N_x Sites on N-Doped Carbon for Aerobic Oxidative Cleavage and Esterification of C(CO)–C Bonds. *Nat. Commun.* **2021**, *12*, 4823.

(22) Zhou, P.; Zhang, Z. One-Pot Reductive Amination of Carbonyl Compounds with Nitro Compounds by Transfer Hydrogenation over Co–N_x as Catalyst. *ChemSusChem* **2017**, *10*, 1892–1897.

(23) Xu, S.; Zhou, P.; Zhang, Z.; Yang, C.; Zhang, B.; Deng, K.; Bottle, S.; Zhu, H. Selective Oxidation of 5-Hydroxymethylfurfural to 2,5-Furandicarboxylic Acid Using O₂ and a Photocatalyst of Co-Thioporphyrazine Bonded to g-C₃N₄. *J. Am. Chem. Soc.* **2017**, *139*, 14775–14782.

(24) Zhang, Z.; Huber, G. W. Catalytic Oxidation of Carbohydrates into Organic Acids and Furan Chemicals. *Chem. Soc. Rev.* **2018**, *47*, 1351–1390.

(25) Zhang, E.; Tao, L.; An, J.; Zhang, J.; Meng, L.; Zheng, X.; Wang, Y.; Li, N.; Du, S.; Zhang, J.; et al. Engineering the Local Atomic Environments of Indium Single-Atom Catalysts for Efficient Electrochemical Production of Hydrogen Peroxide. *Angew. Chem., Int. Ed.* **2022**, *61*, No. e202117347.

(26) Xue, Z.; Luan, D.; Zhang, H.; Lou, X. W. Single-Atom Catalysts for Photocatalytic Energy Conversion. *Joule* **2022**, *6*, 92–133.

- (27) Hai, X.; Xi, S.; Mitchell, S.; Harrath, K.; Xu, H.; Akl, D. F.; Kong, D.; Li, J.; Li, Z.; Sun, T.; et al. Scalable Two-Step Annealing Method for Preparing Ultra-High-Density Single-Atom Catalyst Libraries. *Nat. Nanotechnol.* **2022**, *17*, 174–181.
- (28) Yao, W.; Chen, J.; Wang, Y.; Fang, R.; Qin, Z.; Yang, X.; Chen, L.; Li, Y. Nitrogen-Doped Carbon Composites with Ordered Macropores and Hollow Walls. *Angew. Chem., Int. Ed.* **2021**, *60*, 23729–23734.
- (29) Deng, Q.; Li, X.; Gao, R.; Wang, J.; Zeng, Z.; Zou, J. J.; Deng, S.; Tsang, S. C. E. Hydrogen-Catalyzed Acid Transformation for the Hydration of Alkenes and Epoxy Alkanes over Co–N Frustrated Lewis Pair Surfaces. *J. Am. Chem. Soc.* **2021**, *143*, 21294–21301.
- (30) Wu, W.; Liu, H.; Wu, H.; Zheng, B.; Han, S.; Zhang, K.; Mei, X.; Xu, C.; He, M.; Han, B. Selective Hydrogenolysis of Lignin Model Compounds to Aromatics over a Cobalt Nanoparticle Catalyst. *ACS Sustainable Chem. Eng.* **2021**, *9*, 11862–11871.
- (31) Cook, A.; MacLean, H.; St. Onge, P.; Newman, S. G. Nickel-Catalyzed Reductive Deoxygenation of Diverse C–O Bond-Bearing Functional Groups. *ACS Catal.* **2021**, *11*, 13337–13347.
- (32) Miyamura, H.; Suzuki, A.; Yasukawa, T.; Kobayashi, S. Polysilane-Immobilized Rh–Pt Bimetallic Nanoparticles as Powerful Arene Hydrogenation Catalysts: Synthesis, Reactions Under Batch and Flow Conditions and Reaction Mechanism. *J. Am. Chem. Soc.* **2018**, *140*, 11325–11334.
- (33) Luo, H.; Wang, L.; Shang, S.; Li, G.; Lv, Y.; Gao, S.; Dai, W. Cobalt Nanoparticles-Catalyzed Widely Applicable Successive C–C Bond Cleavage in Alcohols to Access Esters. *Angew. Chem., Int. Ed.* **2020**, *59*, 19268–19274.
- (34) Li, M.; Chen, S.; Jiang, Q.; Chen, Q.; Wang, X.; Yan, Y.; Liu, J.; Lv, C.; Ding, W.; Guo, X. Origin of the Activity of Co–N–C Catalysts for Chemoselective Hydrogenation of Nitroarenes. *ACS Catal.* **2021**, *11*, 3026–3039.
- (35) Nachtigall, O.; VanderWeide, A. I.; Brennessel, W. W.; Jones, W. D. An Iron-Based Dehydration Catalyst for Selective Formation of Styrene. *ACS Catal.* **2021**, *11*, 10885–10891.
- (36) Ding, Y.; Zhu, Z.; Chen, M.; Yu, C.; Zhou, Y. Rhodium-Catalyzed Asymmetric Hydrogenation of All-Carbon Aromatic Rings. *Angew. Chem., Int. Ed.* **2022**, *61*, No. e202205623.
- (37) Murugesan, K.; Senthamarai, T.; Alshammari, A. S.; Altamimi, R. M.; Kreyenschulte, C.; Pohl, M.-M.; Lund, H.; Jagadeesh, R. V.; Beller, M. Cobalt-Nanoparticles Catalyzed Efficient and Selective Hydrogenation of Aromatic Hydrocarbons. *ACS Catal.* **2019**, *9*, 8581–8591.
- (38) Murugesan, K.; Chandrashekar, V. G.; Kreyenschulte, C.; Beller, M.; Jagadeesh, R. V. A General Catalyst Based on Cobalt Core-Shell Nanoparticles for the Hydrogenation of *N*-Heteroarenes Including Pyridines. *Angew. Chem., Int. Ed. Engl.* **2020**, *59*, 17408–17412.
- (39) Ciotonea, C.; Hammi, N.; Dhainaut, J.; Marinova, M.; Ungureanu, A.; El Kadib, A.; Michon, C.; Royer, S. Phyllosilicate-Derived Nickel-Cobalt Bimetallic Nanoparticles for the Catalytic Hydrogenation of Imines, Oximes and *N*-Heteroarenes. *ChemCatChem* **2020**, *12*, 4652–4663.
- (40) Kim, S.; Loose, F.; Bezdek, M. J.; Wang, X.; Chirik, P. J. Hydrogenation of *N*-Heteroarenes Using Rhodium Precatalysts: Reductive Elimination Leads to Formation of Multimetallic Clusters. *J. Am. Chem. Soc.* **2019**, *141*, 17900–17908.
- (41) Stegner, P.; Färber, C.; Zenneck, U.; Knüpfer, C.; Eysel, J.; Wiesinger, M.; Harder, S. Metallic Barium: a Versatile and Efficient Hydrogenation Catalyst. *Angew. Chem., Int. Ed.* **2020**, *60*, 4252–4258.
- (42) Zhang, Z.; Song, J.; Han, B. Catalytic Transformation of Lignocellulose into Chemicals and Fuel Products in Ionic Liquids. *Chem. Rev.* **2017**, *117*, 6834–6880.
- (43) Besson, M.; Gallezot, P.; Pinel, C. Conversion of Biomass into Chemicals over Metal Catalysts. *Chem. Rev.* **2014**, *114*, 1827–1870.
- (44) Turkin, A.; Eyley, S.; Preegel, G.; Thielemans, W.; Makshina, E.; Sels, B. F. How Trace Impurities can Strongly Affect the Hydroconversion of Biobased 5-Hydroxymethylfurfural? *ACS Catal.* **2021**, *11*, 9204–9209.